Southern Ocean CO_2 sink: the contribution of the sea ice

Bruno Delille[1], Martin Vancoppenolle[2], Nicolas-Xavier Geilfus[3] , Bronte Tilbrook[4], Delphine Lannuzel[5,6], Véronique Schoemann[7], Sylvie Becquevort[8], Gauthier Carnat[7], Daniel Delille[9], Christiane Lancelot[7], Lei Chou[10], Gerhard S. Dieckmann[11] and Jean-Louis Tison[7]

[1] *Unité d'Océanographie Chimique, MARE, Université de Liège, Allée du 6 Août, 17, 4000 Liège, Belgium*

[2] *Laboratoire d'Océanographie et du Climat/Institut Pierre-Simon Laplace, CNRS/IRD/UPMC/MNHN, Paris, France*

[3] *Arctic Research Centre, Aarhus University, Aarhus*

[4] *CSIRO Wealth from Oceans National Research Flagship and Antarctic Climate and Ecosystem Cooperative Research Centre, PO Box 1538, Hobart, Australia 7001*[2]

[5] *Antarctic Climate and Ecosystems Cooperative Research Centre, University of Tasmania, Hobart, Australia, PB 80, Hobart, TAS 7001, Australia*

[6] *Institute for Marine and Antarctic Studies, University of Tasmania, Hobart, Australia*

[7] *Glaciology Unit, Department of Earth and Environmental Science, Université Libre de Bruxelles, CP 160/03, 50, Av. F.D. Roosevelt, 1050 Bruxelles, Belgium*

[8] *Ecologie des Systèmes Aquatiques, Université Libre de Bruxelles, Campus de la plaine, CP221, Boulevard du Triomphe, 1050 Bruxelles, Belgium*

[9] *Observatoire Océanologique de Banyuls, Université P. et M. Curie, U.M.R./C.N.R.S. 7621, 66650 Banyuls sur mer, France*

[10] *Laboratoire d'Océanographie Chimique et Géochimie des eaux, Université Libre de Bruxelles, Campus de la plaine, CP208, Boulevard du Triomphe, 1050 Bruxelles, Belgium*

[11] *Alfred-Wegener-Institut fuer Polar- und Meeresforschung, Am Handelshafen 12, 27570 Bremerhaven, Germany*

Key Points

- Antarctic sea ice act as a significant sink for atmospheric CO_2 in spring and summer
- pCO_2 within sea ice brines and related air-ice CO_2 fluxes are strongly related to temperature
- Significance of main sea ice processes on sea-ice CO_2 concentration are assessed and discussed
- In situ measurements were up scaled with the NIMO-LIM3 model

Abstract

We report first direct measurements of the partial pressure of CO_2 (pCO_2) within Antarctic pack sea ice brines and related CO_2 fluxes across the air-ice interface. From late winter to summer, brines encased in the ice change from a CO_2 large over-saturation, relative to the atmosphere, to a marked under-saturation while the underlying oceanic waters remains slightly oversaturated. The decrease from winter to summer of pCO_2 in the brines is driven by dilution with melting ice, dissolution of carbonate crystals and net primary production. As the ice warms, its permeability increases, allowing CO_2 transfer at the air-sea ice interface. The sea ice changes from a transient

source to a sink for atmospheric CO_2. We upscale these observations to the whole Antarctic sea ice cover using the NEMO-LIM3 large-scale sea ice-ocean, and provide first estimates of spring and summer CO_2 uptake from the atmosphere by Antarctic sea ice. Over the spring-summer period, the Antarctic sea ice cover is a net sink of atmospheric CO_2 of 0.029 PgC, about 58% of the estimated annual uptake from the Southern Ocean. Sea ice then contributes significantly to the sink of CO_2 of the Southern Ocean.

Index Terms and Keywords

Sea ice/ Gases/ Biogeochemical cycles, processes, and modelling/ Air/sea interactions/ Carbon cycling/ Arctic and Antarctic oceanography/

Free keywords: sea ice, Antarctic, carbon dioxide, CaCO3 precipitation, NEMO-LIM3

1. Introduction

Climate models often consider sea ice is an inert barrier preventing air-sea exchange of gases, a concept which is presently challenged by observation and theoretical considerations. For decades, sea ice has been assumed to be an impermeable and inert barrier to air-sea exchange of CO_2 so that current assessment of global air-sea CO_2 fluxes or climate models do not include CO_2 exchanges over ice covered waters [*Takahashi et al.*, 2009; *Tison et al.*, 2002].

This paradigm relies on the CO_2 budgets of the water masses of the Weddell Sea. They suggest limited air-sea exchange of CO_2 in the Winter Surface Water when it is subducted and mixed with other water masses to form Weddell Bottom Water [*Poisson and Chen*, 1987; *Weiss*, 1987], a major contributor of Antarctic Bottom Water. However, *Gosink et al.* [1976] showed that sea ice is a highly permeable medium for gases based on work to estimate permeation constants of SF_6 and CO_2 within sea ice. These authors suggested that gas migration through sea ice could be an important factor in winter ocean-atmosphere exchange when the snow-ice interface temperature is above -10°C. Fluxes of CO_2 over sea ice have been reported in the Arctic Ocean [*Geilfus et al.*, 2013; *Geilfus et al.*, 2012; *Miller et al.*, 2011; *Nomura et al.*, 2010; *Nomura et al.*, 2013; *Papakyriakou and Miller*, 2011; *Semiletov et al.*, 2004; *Semiletov et al.*, 2007] and in the Southern Ocean [*Zemmelink et al.*, 2006].

During sea ice growth, most of the impurities (gases, dissolved and particulate matter) are expelled from the pure ice crystals at the ice-water interface (skeletal layer). However, a small fraction of impurities (~10%) remains trapped in gaseous and liquid brine inclusions. These contribute to the overall sea ice porosity and host active auto- and hetero-trophic microbial communities [*Arrigo*, 2003; *Arrigo et al.*, 1997; *Lizotte*, 2001; *Thomas and Dieckmann*, 2002]. Further removal of impurities occurs via brine drainage processes (gravity drainage and flushing) and convection, that are mainly controlled by the history of the thermal regime of the ice [*Eicken*, 2003; *Notz and Worster*, 2009; *Weeks and Ackley*, 1986; *Wettlaufer et al.*, 1997].

Brine volume and salinity adjust to temperature changes in order to maintain thermal equilibrium within the ice [*Cox and Weeks*, 1983]. A 5% relative brine volume is a theoretical threshold above which sea ice permeability for liquid increases drastically

[*Golden et al.*, 1998]. It is also likely to represent a threshold above which air-ice gas exchange increases [*Buckley and Trodahl*, 1987], although Zhou [2013] suggest higher threshold (between 7.5 and 10%) . This permeability threshold would occur at a temperature of -10°C for a bulk ice salinity of 10, corroborating the observation that sea ice is a highly permeable medium for gases [*Gosink et al.*, 1976] allowing air-ice gas exchanges.

The aim of this study is to describe observed pCO_2 and CO_2 fluxes relationships to sea ice temperature from various locations around Antarctica. We assess and compare the relative contribution of biotic and abiotic processes to the observed changes of pCO_2 and estimated related uptake of atmospheric CO_2. Finally we provide a first estimate of Antarctic sea ice contribution to CO_2 exchanges with the atmosphere using two independent methods: a) a global estimate derived from the relative importance of each process controlling the sea ice brine pCO_2 and b) integrating the observed sea ice temperature vs. CO_2 fluxes relationship into a sea ice 3D-model.

2. Material and methods

2.1. Sampling strategy

Measurements were carried out during the 2003/V1 cruise on the *R.V. Aurora Australis* from 2003-09-27 to 2003-10-20 in the Indian sector of the Southern Ocean (63.9 to 65.3 °S, 109.4 to 117.7°E), the ISPOL (Ice Station Polarstern) drift station experiment onboard the *R.V. Polarstern* from 2004-11-29 to 2005-12-31 in the Weddell Sea (67.35 to 68.43 °S, 55.40 to 54.57 °W) and the SIMBA (Sea Ice Mass Balance in the Antarctica) drift station experiment onboard the *R.V. Nathaniel B. Palmer* from 2007-

10-1 to 2007-10-23 in the Bellingshausen Sea (69.51 to 70.45 °S, 94.59 to 92.30 °W). A complete description of these different working stations could be found in *Massom et al.* [2006] for V1, in *Tison et al.* [2008] for ISPOL and in *Lewis et al.* [2011] for SIMBA. Only first year pack ice was investigated during 2003/V1 and SIMBA cruises, while both first year and multiyear pack ice were sampled during ISPOL experiment. Sampling was only carried out in floes without melt ponds or slush surface layers.

pCO_2 of brines

Sampling of ice brine was conducted by drilling shallow sackholes (ranging from 15 cm down to almost full ice thickness) through the surface of the ice sheet. The brine from adjacent brine channels and pockets was allowed to seep into the sackhole for 30-60 min, with the hole covered with a plastic lid [*Gleitz et al.*, 1995], reportedly the best current method to sample brines for chemical studies [*Papadimitriou et al.*, 2004]. Brines was pumped from the hole using a peristaltic pump (Masterflex® - Environmental Sampler), supplied to the device for measurements of partial pressure of CO_2 (pCO_2) and recycled back at the bottom of the sackhole. The latter were carried out using a membrane contractor equilibrator (Membrana® Liqui-cell) coupled to an infrared gas analyzer (IRGA, Li-Cor® 6262). Seawater or brines flowed into the equilibrator at a maximum rate of 1 L min^{-1} and a closed air loop ensured circulation through the equilibrator and the IRGA at a rate of 3 L min^{-1}. Temperature was measured simultaneously *in situ* and at the outlet of the equilibrator using Li-Cor® sensors. Temperature correction of pCO_2 was applied assuming that the relation from Copin-Montégut [1988] is valid at low temperature and high salinity. The IRGA was calibrated soon after returning to the ship while the analyser was still cold. For V3/2001, CO_2-in-air standards calibrated on the World Meteorological Organisation X-85 molar scale

(mixing ratios of 304.60, 324.65 and 380.03 ppm) were supplied by Commonwealth Scientific and Industrial Research Organisation (CSIRO) Atmospheric Research, Australia. CO_2-in-air standards with mixing ratios of 0 ppm and 350 ppm of CO_2 were supplied by Air Liquide Belgium® for the ISPOL and SIMBA cruise. Stable field pCO_2 readings usually occurred within 3 min of flowing gas into the IRGA. The equilibration system ran 6 min before averaging the values given by the IRGA and temperature sensors over 30 s and recording the averaged values with a data logger (Li-Cor® Li-1400). All the devices (except the peristaltic pump) were enclosed in an insulated box containing a 12V power source and was warmed to keep the inside temperature just above 0°C.

2.2. Dissolved inorganic carbon and total alkalinity

A peristaltic pump (Masterflex® - Environmental Sampler) was used to collect brines from sackholes but also underlying water at the ice-water interface, 30 m deep and at an intermediate depth (5 m during 2003/V1 cruise and 1 m during ISPOL cruise) for dissolved inorganic carbon (DIC) and total alkalinity (TA) measurements.

DIC measurements on 2003/V1 were made using a single operator multiparameter metabolic analyzer (SOMMA) and UIC® 5011 coulometer [*Johnson et al.*, 1998]. The system was calibrated by injecting known amounts of pure CO_2 into the system. The number of moles of pure CO_2 injected bracketed the amounts measured in sea ice brines and showed the measurement calibration did not change over the range of concentrations measured. The measurement precision and accuracy was checked during the analyses using certified reference materials provided by Dr A Dickson, Scripps

Institution of Oceanography. Repeat analyses showed an accuracy and precision for the DIC measurements better than ±0.1%.

TA was computed from pCO_2 and DIC using the CO_2 dissociation constants of *Mehrbach et al.* [1973] refitted by [*Dickson and Millero,* 1987]. We assumed a conservative behaviour of dissociation constants during seawater freezing.. During the ISPOL experiment, TA was measured using the classical Gran potentiometric method [*Gran*, 1952] on 100-mL GF/C filtered samples, with a reproducibility of ±3 µmol kg^{-1}. DIC was computed from TA and pCO_2 for ISPOL.

2.3. Air-ice CO_2 fluxes

A chamber was used to measure air-ice CO_2 fluxes. The accumulation chamber (West system®) is a metal cylinder closed at the top (internal diameter 20 cm; internal height 9.7 cm) with a pressure compensation device. A rubber seal surrounded by a serrated-edge iron ring ensured an air-tight connection between the base of the chamber and the ice. For measurement over snow, an iron cylinder was mounted at the base of the chamber to enclose snow down to the ice and prevent lateral advection of air through the snow. The chamber was connected in a closed loop between the air pump (3 L min^{-1}) and the IRGA. The measurement of pCO_2 in the chamber was recorded every 30 s for at least 5 min. The flux was computed from the slope of the linear regression of pCO_2 against time ($r^2 \geq \pm 0.99$) according to *Frankignoulle* [1988]. The uncertainty of the flux computation due to the standard error on the regression slope is on average ±3%.

2.4. Air-ice CO_2 flux/ice temperature relationship

Using field data, we calculated a relationship between CO_2 fluxes (F_{CO2}) over both first year and multiyear ice as a function of sea ice temperature (T_{si}) at 5cm depth (fig. 1a). The regression is composed of two second-order polynomial regressions valid between -9°C and -7°C and between -7°C and 0°C, respectively (table 1).

2.5. Description of the sea ice model

We used NEMO-LIM3 [*Madec*, 2008; *Vancoppenolle et al.*, 2008] ocean-sea ice model to scale *in-situ* measurements. NEMO (Nucleus for European Modelling of the Ocean) is a widely used ocean model, while LIM3 (Louvain-la-Neuve Ice Model) is an advanced large-scale sea ice model, carefully validated for both hemispheres. LIM3 is a C-grid dynamic thermodynamic model, including the representation of the subgrid-scale distributions of ice thickness, enthalpy and salinity as well as snow volume. Ice dynamics are resolved using an elasto-visco-plastic rheology, following concepts of Hunke and Dukowicz [1997]. Snow and sea ice thermodynamics include vertical diffusion of heat with a formulation of brine thermal effect. There is also an explicit formulation of brine entrapment and drainage. Sources and sinks of ice mass include basal growth and melt, surface melt, new ice formation in open water, as well as snow ice formation. In order to account for subgrid-scale variations in ice thickness, ice volume and area are split into 5 categories of ice thickness. Thermodynamic (ice growth and melt) as well as dynamical (rafting and ridging) processes control the redistribution of ice state variables within the ice thickness categories. LIM3 is coupled to NEMO, a hydrostatic, primitive equation finite difference ocean model running on a $2°\times2°\cos\phi$ grid called ORCA2.

We used the NEMO-LIM3 model output rather than satellite derivations of sea ice temperature as the latter are presently not reliable in all conditions [*Lewis*, 2010]. In comparison, we have reasonable confidence in the ice thickness, snow depth and temperature simulated by LIM3, for the two following reasons. Firstly, a series of one-dimensional validations of the thermodynamic component of LIM3 was made over various sites in both hemispheres [*Vancoppenolle et al.*, 2007]. Vertical profiles of temperature, salinity, as well as ice thickness and snow depth were found to be in close agreement with field observations. In particular, the sea ice permeability transitions seem to be quite well captured. Secondly, an extensive large-scale validation of LIM3, forced by NCEP-NCAR daily reanalyses of meteorological data [*Kalnay et al.*, 1996] was performed [*Vancoppenolle et al.*, 2008]. In the Antarctic, the simulated sea ice concentration, thickness, drift and salinity and snow depth model fields are in reasonable agreement with available observations. Because of errors in the wind forcing, there is a low bias in ice thickness along the East side of the Antarctic Peninsula, but this region is not of particular importance for the present analysis.

2.6. Computation of the snow-ice interface temperature and air-ice CO_2 flux in the sea ice model.

In LIM3 (fig. 2), for each model grid cell, the sea ice thickness categories have a relative coverage a^l (l = 1, …, 5). In each thickness category *l*, the sea ice is treated as a horizontally uniform column with ice thickness h_i^l and snow depth h_s^l. In order to compute the vertical temperature profile, the sea ice in each category is vertically divided into one layer of snow, with a midpoint temperature T_s and N=5 layers of sea

231 ice with midpoint temperatures T_i^{kl} (k = 1, …, 5). The snow and sea ice temperatures
232 are computed by the model by solving the heat diffusion equation. For the purpose of
233 the present study, we diagnose the ice-air interfacial temperature by assuming the
234 continuity of the heat conduction flux at the snow-ice interface:

235 $$T_{si} = \frac{k_i^1 T_i^1 h_s + k_s T_s h_i / N}{k_i^1 h_s + k_s h_i / N}, \quad (1)$$

236 where k_i^1 and k_s are the thermal conductivities of the first sea ice layer and of snow,
237 respectively. The latter is done for each sea ice thickness category, which gives T^l_{si} (l=1,
238 …, 5).
239 The temperature at the snow-ice interface (fig. 1b) is used to compute the air-ice CO_2
240 flux in each sea ice thickness category, using the empirical relationship of
241 The fFigure 1b:

242 $$F_{CO2}^l = F_{CO2}(T_{si}^l). \quad (2)$$

243 Finally, the net, air-ice CO_2 flux over all ice categories in the model grid cell is given
244 by:
245

246 $$F_{CO2}^{air-ice} = \sum_{l=1}^{5} a_i^l F_{CO2}^l . \quad (3)$$

247 Note that, as flooding affects the CO_2 dynamics, points with surface flooding were
248 excluded in the present analysis. Snow-ice formation occurs in the model if the snow
249 load is large enough to depress the snow-ice interface under the sea level. The flooded
250 snow is transformed into ice by applying heat and mass conservation.
251 Following the setup detailed in *Vancoppenolle et al.* [2008], we conducted a hindcast
252 simulation of the Antarctic sea ice pack over 1976-2007, using a combination of daily
253 NCEP reanalyses of air temperature and winds [*Kalnay et al.*, 1996] and of various

254 climatologies to compute the thermodynamic and dynamic forcings of the model. In
255 addition, the simulation includes the diagnostic air-ice CO_2 flux. The time step is 1.6 h
256 for the ocean and 8 h for the sea ice.
257

258 # 3. Results and discussion

259 ## 3.1. Changes in pCO_2 of brines and air-ice CO_2 fluxes during sea ice warming

260 ### 3.1.1. pCO_2 of brines

261 Sea ice-brine pCO_2 decreased dramatically as sea ice warmed (fig. 1a) and the brines
262 shifted from a large CO_2 over-saturation ($\Delta pCO_2 = pCO_{2(brines)} - pCO_{2(air)} =$ 525ppm)
263 during early spring (October) to a marked under-saturation (ΔpCO_2 = -335 ppm) during
264 summer (December). The sea ice brine pCO_2 appears to be tightly related to sea ice
265 temperature.

266 As the ice temperature increases, ice crystals melt and salinity decreases accordingly.
267 We explored the relationships among brine pCO_2, temperature and salinity by carrying
268 out a step-wise simulation of conservative dilution of early spring-time brine collected
269 during 2003/V1 cruise during warming at thermal brine-ice equilibrium. In details, (i)
270 we calculated brine salinity at a given temperature according to the relationship of *Cox*
271 *and Weeks* [1983]; (ii) we normalized mean TA and DIC to a salinity of 35 (TA_{35}, and
272 DIC_{35}, respectively) for the two coldest brines collected during 2003/V1 cruise; (iii) we
273 computed TA_t and DIC_t at a given temperature, t (and related salinity) assuming a
274 conservative behaviour of TA and DIC; and (iv) computed the brine pCO_2 for each
275 temperature from TA_t and DIC_t, using CO_2 acidity constants of *Dickson and Millero*

276 [1987]. Here we assume that these constants are valid for the range of temperatures and
277 salinities encountered within the sea ice [*Delille et al.*, 2007; *Papadimitriou et al.*,
278 2004]. The resulting pCO_2 - temperature relationship is shown in fig. 1a (red dashed
279 curve). The dilution effect largely encompasses the thermodynamic effect of
280 temperature increase on pCO_2 and the pattern of observed pCO_2 matches the theoretical
281 variation related to both processes. This suggests that a large part of the spring pCO_2
282 drawdown is driven by the dilution of brines associated with the melting of ice crystals
283 as temperature increases. Conversely, the over-saturation observed at the end of winter
284 can result from brine concentration during sea ice growth and cooling.

285 **3.1.2.CO_2 fluxes**

286 While air-ice CO_2 fluxes were not detectable below -8°C (fig. 1b) , we observed
287 positive fluxes up to +1.9 mmol m^{-2} d^{-1} between -8 and -6 °C (where a positive flux
288 corresponds to a release of CO_2 from the ice to the atmosphere). Above -6°C, air-ice
289 CO_2 fluxes decrease down to –5.2 mmol m^{-2} d^{-1} in parallel with the increase of
290 temperature. These fluxes are of the same order of magnitude as the fluxes reported by
291 *Nomura et al.* [2013] over land fast ice. Higher sinks (negative fluxes:-6.6 to -18.2
292 mmol m^{-2} d^{-1}) have been reported in Antarctica [*Zemmelink et al.*, 2006]. These were
293 carried out using eddy covariance over a slush ice - a mixture of melting snow, ice and
294 flooding seawater covering the sea ice. Note, however, that computations of *Zemmelink*
295 *et al.* [2006] should be considered with caution, since they did not take into account at
296 the time proper corrections required for open-path CO_2 analyser in cold temperature
297 [*Burba et al.*, 2008].

3.2. Assessment of atmospheric CO_2 uptake by Antarctic sea ice from the relative contribution of processes controlling sea ice pCO2

Impurities expulsion (that might be enhanced for CO_2 compared to salt [*Loose et al.*, 2009]), changes in brines concentration, precipitation or dissolution of carbonate [*Anderson and Jones*, 1985; *Delille et al.*, 2007; *Papadimitriou et al.*, 2004; *Papadimitriou et al.*, 2007; *Rysgaard et al.*, 2007], abiotic release or uptake of gaseous CO_2, primary production and respiration all contribute to CO_2 dynamics [*Delille et al.*, 2007; *Søgaard et al.*, 2013] in sea ice. In this section we will describe those processes and provide an estimate of their relative contribution to spring and summer pCO_2 changes in sea ice. We estimated the potential maximal individual impact of thermodynamic, chemical and biological processes (temperature increase and related dilution, carbonate dissolution and primary production) to the spring-summer decrease of pCO_2 (table 2). The variations are computed from the conditions of temperature, bulk ice salinity, TA_{35} and pCO_2 (-7.2°, 5.4, 791 µmol kg^{-1}, 724 ppm, respectively) corresponding to the average of the two coldest conditions encountered during the 2003/V1 (coldest end term of the solid curve in figure 1a) and ISPOL cruises. Related changes during the spring to summer transition are discussed in the sections below.

3.3. Changes in brines concentration

In autumn and winter, decrease of temperature leads to the concentration of solutes in brines inclusions which induce high pCO_2 within sea ice brines as observed in figure 1a. In spring and summer, as the temperature increases, the melt of ice crystals and the subsequent dilution of the brines promote a decrease of the sea ice brine pCO_2. For all our cruises, temperature increased from -7.2 °C to -1.3°C (corresponding to an increase of 5.9°C in table Table 1: Fit expression of the relationship between CO2 fluxes (FCO2) over both first year and multiyear ice as a function of sea ice temperature (Tsi) at 5cm

depth used for reconstructing air-ice CO2 fluxes from the NEMO-LIM3 model as it appears in figure 1b (solid curve). Number of samples, mean error, standard error, root-mean-square error, coefficient of determination were 21, -0.099 mmol C m-2 d-1, 0.995 mmol C m-2 d-1, 0.953, 0.728, respectively.

Tsi (°C)	FCO2 (mmol C m-2 d-1)
Tsi < -9	0
-9 < Tsi< -7	FCO2=27.945 + 6.39 Tsi + 0.365 Tsi2
Tsi > -7	FCO2=-4.41962 - 0.54286 Tsi 0.035 Tsi2

Table 2) with a decrease of the brine salinity from 117.1 to 23.5, (corresponding to a salinity change of -94 in table Table 1: Fit expression of the relationship between CO2 fluxes (FCO2) over both first year and multiyear ice as a function of sea ice temperature (Tsi) at 5cm depth used for reconstructing air-ice CO2 fluxes from the NEMO-LIM3 model as it appears in figure 1b (solid curve). Number of samples, mean error, standard error, root-mean-square error, coefficient of determination were 21, -0.099 mmol C m-2 d-1, 0.995 mmol C m-2 d-1, 0.953, 0.728, respectively.

Tsi (°C)	FCO2 (mmol C m-2 d-1)
Tsi < -9	0
-9 < Tsi< -7	FCO2=27.945 + 6.39 Tsi + 0.365 Tsi2
Tsi > -7	FCO2=-4.41962 - 0.54286 Tsi 0.035 Tsi2

Table 2) according to relationships of Cox and Weeks [1983].

The decrease in salinity, related to the rise of temperature, leads to the dilution of DIC and TA. This induces a computed pCO_2 drop of 684 ppm (table Table 1: Fit expression of the relationship between CO2 fluxes (FCO2) over both first year and multiyear ice as a function of sea ice temperature (Tsi) at 5cm depth used for reconstructing air-ice CO2 fluxes from the NEMO-LIM3 model as it appears in figure 1b (solid curve). Number of samples, mean error, standard error, root-mean-square error, coefficient of determination were 21, -0.099 mmol C m-2 d-1, 0.995 mmol C m-2 d-1, 0.953, 0.728, respectively.

Tsi (°C)	FCO2 (mmol C m-2 d-1)
Tsi < -9	0
-9 < Tsi< -7	FCO2=27.945 + 6.39 Tsi + 0.365 Tsi2
Tsi > -7	FCO2=-4.41962 - 0.54286 Tsi 0.035 Tsi2

Table 2), using the CO_2 dissociation constants of *Mehrbach et al.* [1973] refitted by *Dickson and Millero* [1987]. Brine dilution by internal melting appears to account for a significant part of the observed pCO_2 spring drawdown.

3.4. Primary production

356 While sympagic algae are still active in autumn and winter, their photosynthetic rate
357 should be limited by light availability, low temperatures, high salinity and restricted
358 space for growth [*Arrigo et al.*, 1997; *Mock*, 2002], and this contribution to the DIC
359 normalized to a constant salinity of 35 (DIC_{35}) winter removal observed in the figure 3
360 is therefore likely small.

361 Estimating primary production in sea ice – and the related impact on pCO_2 - is
362 challenging. We assumed the overall sea ice primary production prior to and during the
363 ISPOL cruise corresponded to the autotrophic organic carbon ($OC_{autotroph}$) standing stock
364 in the ice at the end of the ISPOL cruise. This autotrophic organic carbon was estimated
365 from Chl *a* measurements (at 6 depths) presented in [*Lannuzel et al.*, 2013] and a
366 C:Chla ratio of 83. This ratio was determined by comparing Chl *a* concentration and
367 $OC_{autotroph}$ content derived from abundance and biovolume of autotrophic organisms
368 measured from inverted and epifluorescence microscopy observations, and
369 carbon:volume conversion factors [*Hillebrand et al.*, 1999; *Menden-Deuer and Lessard*,
370 2000].
371 The autotrophic organic carbon amount could be underestimated because it does not
372 take into account losses of autotrophic organic carbon (i.e. mortality, exchange with the
373 underlying seawater). On the other hand, we neglected the part of autotrophic
374 community originating from organisms trapped during sea ice growth and autumnal
375 primary production. At the end of the ISPOL cruise, the mean Chl *a* concentration was
376 3.7 µg kg^{-1} of bulk ice, which corresponds to an $OC_{autotroph}$ standing stock of 309 µgC
377 kg^{-1} of bulk ice. The build up of the $OC_{autotroph}$ standing stock would correspond to an
378 uptake of DIC of 25.8 µmol kg^{-1} in bulk ice and an increase of TA of 4.1 µmol kg^{-1} of
379 bulk ice, according to the Redfield-Ketchum-Richards stoichiometry of biosynthesis

[*Redfield et al.*, 1963; *Richards*, 1965]. With the volume of brines derived from the equations of Cox and Weeks [1975], revisited by Eicken [2003], this leads to a DIC decrease of 669 µmol kg^{-1} of brines and a TA increase of 107 µmol kg^{-1} of brines (table 2) and a subsequent decrease of the of brines pCO_2 of 639 ppm (table 2**).** The build up of the $OC_{autotroph}$ standing stock would also correspond to a primary production of 0.26 gC m^{-2} considering an ice thickness of 90 cm (average ice thickness during the ISPOL survey).

3.5. Calcium carbonate

The figure 3 provides insights on the processes occurring within sea ice prior and during our surveys. We plotted normalized DIC_{35} versus normalized TA (TA_{35}) in order to distinguish which processes, other than dilution/concentration and temperature changes, control the carbonate system. Normalization removes the influence of dilution/concentration, while temperature changes do not affect DIC and TA. The biogeochemical processes that can potentially affect DIC_{35} and TA_{35} are reported as solid bars. TA_{35} and DIC_{35} of brines in spring are significantly lower than in the underlying water. Differences between brines and the underlying water decrease in summer. TA_{35} and DIC_{35} in both spring and summer are remarkably well correlated with a slope of 1.2. Carbonate dissolution/precipitation best explain the observed trend, although the theoretical slope should be 2. Such a discrepancy might be due to uptake of gaseous CO_2 (from bubbles or the atmosphere) combined with carbonate dissolution, mixing with underlying water owing to internal convection, or enhanced gas expulsion [*Golden et al.*, 1998; *Loose et al.*, 2009; *Weeks and Ackley*, 1986] . The low TA_{35} value

403 observed during 2003/V1 cruise suggests that carbonate precipitation occurred within
404 sea ice prior to the cruise.

405 *Rysgaard et al.* [2007] suggested that precipitation of calcium carbonate in sea ice can
406 act as a significant sink for atmospheric CO_2. However, there are still some crucial gaps
407 in the current understanding of carbonate precipitation in sea ice. In particular available
408 field experiments hardly addressed the timing and conditions of carbonate precipitation
409 in natural sea ice. Knowing these conditions is nevertheless crucial to assess the role
410 played by sea ice carbonate precipitation as a sink or source of CO_2 for the atmosphere.
411 In order to bring some attention on the need to better constrain $CaCO_3$ precipitation in
412 natural sea ice, we consider below different scenarios of $CaCO_3$ precipitation and
413 explore how air-ice CO_2 fluxes depend on the condition of $CaCO_3$ precipitation.
414 Furthermore, the fate of carbonate precipitates is a good illustration of how intricate the
415 links between biogeochemical and physical sea ice processes are (fig. 4). Based on field
416 studies, "excess" TA in the water column during sea ice melting was attributed to the
417 dissolution of calcium carbonate precipitated in brines and released into the underlying
418 water [*Jones et al.*, 1983; *Rysgaard et al.*, 2007]. Precipitation of calcium carbonate as
419 ikaite ($CaCO_3.6H_2O$) crystals have been observed both in the Arctic and the Antarctic
420 sea ice [*Dieckmann et al.*, 2008; *Dieckmann et al.*, 2010; *Geilfus et al.*, 2013; *Rysgaard*
421 *et al.*, 2007; *Rysgaard et al.*, 2013; *Søgaard et al.*, 2013].
422 If carbonate precipitate in high salinity – low temperature conditions, such precipitation
423 would likely take place in late autumn or winter in the upper layers of sea ice while
424 brines channels are closed (fig. 4B). This precipitation produces CO_2. If brines channels
425 are closed, this CO_2 is not transported elsewhere. For instance *Killawee et al.* [1998]
426 and *Tison et al.* [2002] already observed CO_2 rich bubbles in artificial sea ice and

427 suggested that they could be issued from carbonate precipitation. During spring internal
428 melting, dissolution of carbonate solids formed in fall and winter should consumes CO_2
429 in the same amount as it was produced by precipitation. The net uptake of
430 atmospheric/sea water CO_2 related to the production and dissolution of carbonate in that
431 case would be nil over the period.
432 In the opposite, the phase diagram of *Assur* [1958] and the work of *Richardson* [1976],
433 suggest that ikaite could precipitate at relatively high temperature (-2.2°C) and low
434 salinity. Under these conditions, carbonate precipitation might potentially take place in
435 the skeletal layer (the lamellar ice-water interface, a relatively open system) during sea
436 ice growth (fig. 4F). At the ice-water interface, the segregation of impurities enhances
437 CO_2 concentration at the ice-water interface during ice growth [*Killawee et al.*, 1998]
438 and acts as a source of CO_2 for the underlying layer. CO_2 produced by the precipitation
439 can either be expelled to the underlying water layer (fig. 4C) or released to the
440 atmosphere, especially in young thin permeable sea ice [*Geilfus et al.*, 2013]. A crucial
441 issue is the fate of carbonate solids formed in the skeletal layer. They can either a) sink
442 (fig. 4F) in the underlying layer faster than the CO_2 rich brines (fig. 4 D). In that case,
443 carbonate precipitation act as a net source of CO_2 for the atmosphere, especially if some
444 CO_2 rich brines trapped within sea ice are connected to the atmosphere in spring and
445 summer (fig. 4E). b) Carbonate solids may sink at the same rate than the brines that
446 transport produced CO_2 with negligible impact on DIC budget of the water column and
447 the impact for the atmosphere is nil. c) Carbonate solids remain trapped in the tortuosity
448 of the skeletal layer while CO_2 produced by the precipitation is expelled to the
449 underlying water with the brines (fig. 4 C) and entrained towards deep layers due to the
450 high density of brines. The dissolution of trapped carbonate solids in spring and summer

451 triggered by temperature increases and related salinity decreases, would consume CO_2
452 and drive CO_2 uptake within the ice. In that case carbonate precipitation acts as a sink
453 for atmospheric CO_2. However *Papadimitriou et al.* [2013] showed recently that at -
454 2.2°C carbonate precipitation can occur only in low pCO_2 conditions, that are
455 uncommon below sea ice during sea ice formation.
456 Taking into account the estimates of the saturation state of ikaite as a function of brine
457 pCO_2 and temperature provided by *Papadimitriou et al.* [2013] and taking into account
458 the pCO_2 vs temperature relationship of the figure 1a, it seems reasonable that the
459 threshold of saturation of ikaite for brine corresponds to temperature ranging between -
460 5°C and -6°C. So when the ice cools down, carbonate precipitation can potentially
461 develop below -5°C. If the bulk salinity of ice is above 5, then at -5°C, the brine volume
462 is above 5% [*Cox and Weeks*, 1983; *Eicken*, 2003] and ice is permeable [*Golden et al.*,
463 1998]. In these conditions, fluids still percolate and transport CO_2 while solid particles
464 remain trapped due to the tortuosity of the ice matrix. This corresponds to the previous
465 (c) scenario.
466 This leads to the segregation between carbonate precipitates, which remain trapped
467 within sea ice while the CO_2 produced is expelled to the underlying water with brines.
468 Such a mechanism could act as an efficient pump of CO_2 from the atmosphere. The
469 expulsion of brines enriched in CO_2 leads to the formation of dense water that sinks
470 rapidly during sea ice growth. The sinking of dense water is the main driver of deep-
471 water formation and is potentially an efficient CO_2 sequestration pathway. Numerous
472 vertical distributions profiles of TA below sea ice have revealed the signature of
473 carbonate precipitation [*Weiss et al.*, 1979]. When sea ice melts during spring and
474 summer, trapped carbonate solids dissolve as the result of the combined increase of

475 temperature and decrease of salinity either within sea ice or in the underlying water.
476 This dissolution of carbonate solids observed by *Jones et al.* [1983] leads to a decrease
477 of pCO_2 and might act as an efficient and significant sink of CO_2 according to
478 observations and models [*Rysgaard et al.*, 2011; *Rysgaard et al.*, 2012; 2007; *Søgaard*
479 *et al.*, 2013]. However, as underlined before, part of that process might not be a net
480 annual sink if carbonate precipitate in permeable sea ice, and that the produced CO_2
481 degasses to the atmosphere [*Geilfus et al.*, 2013].
482 Low values of DIC_{35} and TA_{35} in brines collected in early spring in cold sea ice (fig. 3)
483 indicate that carbonate precipitation occurred within brines prior to the 2003/V1 cruise,
484 further eastwards. The imprint of carbonate precipitation is well marked, leading to a
485 decrease of 65 % of TA_{35} in brines, compared to the underlying water (fig. 3). Such
486 difference would correspond to the precipitation of carbonate of about 2038 µmol kg^{-1}
487 from the brines, assuming the effect of fall and winter microbial activity on TA is
488 negligible. Carbonate precipitation will reduce the DIC_{35} and increase pCO_2 as the brine
489 salinity increases during ice growth. This will contribute to the winter over-saturation of
490 CO_2. If we assume that the carbonate solids remain trapped within the ice and no CO_2 is
491 stored in the gaseous phase within sea ice during the cooling processes, then spring
492 dissolution would reduce pCO_2 by about 583 ppm (table Table 1: Fit expression of the
493 relationship between CO2 fluxes (FCO2) over both first year and multiyear ice as a
494 function of sea ice temperature (Tsi) at 5cm depth used for reconstructing air-ice CO2
495 fluxes from the NEMO-LIM3 model as it appears in figure 1b (solid curve). Number of
496 samples, mean error, standard error, root-mean-square error, coefficient of
497 determination were 21, -0.099 mmol C m-2 d-1, 0.995 mmol C m-2 d-1, 0.953, 0.728,
498 respectively.

Tsi (°C)	FCO2 (mmol C m-2 d-1)
Tsi < -9	0
-9 < Tsi< -7	FCO2=27.945 + 6.39 Tsi + 0.365 Tsi2
Tsi > -7	FCO2=-4.41962 - 0.54286 Tsi 0.035 Tsi2

499

500

501

502 Table 2).

503 However, the observed decrease in TA_{35} due to carbonate precipitation corresponds
504 theoretically to a removal of 30 % of $DIC_{35,}$ while the overall decrease of DIC_{35} reaches
505 70% at the coldest temperature (fig. 3). Thus, about 40% of DIC_{35} reduction has to be
506 ascribed to either autumnal/winter primary production or CO_2 transfer to the gas phase
507 within the brines or enhanced gas expulsion compared to salt [*Loose et al.*, 2009]. For
508 instance, *Geilfus et al.* [2013] report significant release of CO_2 from the ice to the
509 atmosphere as a result of solutes expulsion during early stages of ice formation.

510 **3.6. First order assessment of air-ice CO_2 transfers over Antarctic sea ice**

511 The potential air-ice CO_2 transfers related to sea ice physical and biogeochemical
512 processes were assessed by considering a homogeneous 90 cm thick sea ice cover in
513 equilibrium with the atmosphere and isolated from exchange with the underlying water.
514 The sea ice thickness value is the mean observed during the ISPOL experiment and is
515 low compared to the values generally observed in the Weddell Sea and elsewhere [*Haas*
516 *et al.*, 2003; *Timmermann et al.*, 2002]. Temperature, salinity and $\delta^{18}O$ data [*Tison et*
517 *al.*, 2008] suggest that low exchanges occurred between sea ice and the underlying layer

518 during the ISPOL experiment . We assumed that sea ice was initially in equilibrium
519 with the atmosphere (pCO_2 = 370 ppm), and we applied the biogeochemically driven
520 DIC and TA changes of table Table 1: Fit expression of the relationship between CO2
521 fluxes (FCO2) over both first year and multiyear ice as a function of sea ice temperature
522 (Tsi) at 5cm depth used for reconstructing air-ice CO2 fluxes from the NEMO-LIM3
523 model as it appears in figure 1b (solid curve). Number of samples, mean error, standard
524 error, root-mean-square error, coefficient of determination were 21, -0.099 mmol C m-2
525 d-1, 0.995 mmol C m-2 d-1, 0.953, 0.728, respectively.

Tsi (°C)	FCO2 (mmol C m-2 d-1)
Tsi < -9	0
-9 < Tsi< -7	FCO2=27.945 + 6.39 Tsi + 0.365 Tsi2
Tsi > -7	FCO2=-4.41962 - 0.54286 Tsi 0.035 Tsi2

526

527

528

529 Table 2 (expressed per kilogram of bulk ice), and then computed the air-ice CO_2
530 transfers required to restore equilibrium. We used the brine volume values computed
531 from the equations of *Cox and Weeks* [1975] revisited by *Eicken* [2003] and mean
532 conditions observed during the two last ISPOL stations (mean sea ice temperature: -
533 1.3°C, mean brine salinity: 24, mean bulk ice salinity: 3.8, mean TA: 1667 µmol kg^{-1} of
534 brines). For the uptake owing to temperature change and related dilution effect, we
535 considered a temperature increase from -7.2 to -1.3 °C corresponding to the range of
536 observations during the 2003/V1 and ISPOL cruises, salinity decrease from 117 to 24

537 and decrease of TA from 8135 to 1667 µmol kg^{-1} of brines so that TA_{35} remains
538 constant.
539 For an Antarctic first-year sea ice surface area of 14×10^6 km^2 [*Comiso*, 2003], the
540 corresponding upscaled overall CO_2 uptake due to those cumulated three processes
541 (table 3) is 0.024 PgC for Spring-Summer.

542 **3.7. Comparison of the significance of the main processes on CO_2 uptake**

543 Tables 2 and 3 provide some insights on the relative contribution of the three main
544 processes (increase of temperature and related dilution, primary production and
545 dissolution of carbonate solids) to the pCO_2 drawdown and the uptake of atmospheric
546 CO_2. It must keep in mind that the assessment of the contribution of primary production
547 is less robust than the other assessments. As observed by *Delille et al.* [2007] in
548 Antarctic land fast ice, the impact on pCO_2 of warming and related dilution is similar to
549 those of dissolution of carbonate solids. The contribution of primary production is only
550 slightly lower (tables 2). In terms of CO_2 uptake, the contribution of primary production
551 represents only 45 % of the contribution of each other process, but it still significant. In
552 contrast *Søgaard et al.* [2013] in subarctic land fast suggest that the contribution of
553 primary production to the uptake of atmospheric CO_2 is pretty small compare to the
554 other processes. However, these differences should reflect the differences in primary
555 production between different areas.
556

557 **3.8. Assessment of atmospheric CO_2 uptake by Antarctic sea ice from fluxes:sea ice**
558 **temperature relationship in a 3D model.**

559 We measured CO_2 fluxes over widespread sea ice without biologically active surface
560 communities. Previous eddy correlation CO_2 fluxes measurements were carried out over

561 areas covered by particular surface environments, namely melt ponds and slush
562 [*Semiletov et al.*, 2004; *Zemmelink et al.*, 2006]. Slush is known to hosts a highly
563 productive algae community [*Legendre et al.*, 1992]. Sea ice surface communities
564 benefit from high light levels and from nutrients from seawater flooding as snow
565 loading or sea ice rafting depress the ice surface below the freeboard. Such surface
566 flooding occurs over 15-30% of the ice pack in Antarctica [*Wadhams et al.*, 1987].
567 These surface communities exhibit photosynthetic rates comparable to those of open
568 ocean Antarctic phytoplankton [*Lizotte and Sullivan*, 1992] and might be responsible for
569 the majority of sea surface productivity in Antarctic sea ice [*Legendre et al.*, 1992].
570 They easily exchange CO_2 with the atmosphere through the porous snow cover and can
571 potentially enhance significantly the estimate for CO_2 uptake by the sea ice cover given
572 below.
573 In a heterogeneous environment like sea ice, the small spatial resolution of the chamber
574 CO_2 flux measurements allows a consistent comparison with pCO_2 within the ice. The
575 pCO_2 gradient between the atmosphere and the brines in the sea ice top layer is the main
576 driver of CO_2 fluxes. The CO_2 fluxes are consistent with the saturation level of CO_2 in
577 the brines. No CO_2 flux was detected below -10°C suggesting that sea ice was then
578 virtually impermeable to CO_2 exchange (fig. 1b). At a temperature of ~ -7°C, the low
579 permeability of the ice results in weak net CO_2 fluxes despite elevated pCO_2. As the
580 temperature increases, pCO_2 of the ice decreases and sea ice shifts from a transient CO_2
581 source to a sink.
582 The fluxes are modulated by factors like sea ice temperature, and snow and ice structure
583 [*Geilfus et al.*, 2012; *Nomura et al.*, 2010; *Nomura et al.*, 2013]. While snow allows
584 exchange of gases with the atmosphere [*Albert et al.*, 2002; *Massman et al.*, 1997;

585 *Takagi et al.*, 2005], very low to nil fluxes were observed after the formation of lenses
586 of superimposed ice above sea ice (diamonds in figure 1b) that was detected at the
587 sampling site and elsewhere during ISPOL cruise [*Nicolaus et al.*, 2009]. Superimposed
588 ice forms after a strong snow melt event when percolating freshwater refreezes at the
589 contact of proper sea ice [*Haas et al.*, 2001]. As freshwater ice, the superimposed ice is
590 impermeable to gas transport [*Albert and Perron*, 2000]. The formation of
591 superimposed ice at the top of sea ice observed at certain stations during ISPOL cruise
592 is the best candidate to explain the inhibition of air-ice CO_2 fluxes at those stations.
593 During superimposed ice events, ongoing strong dilution of the brine by the melting sea
594 ice was decreasing brine pCO_2. Development of superimposed ice impeded CO_2 transfer
595 from the atmosphere to the sea ice that normally should drive pCO_2 values toward the
596 atmospheric concentration. As a result drastic decreases of brine pCO_2 down to 30 ppm
597 were observed during superimposed ice events. This highlights the role of CO_2 invasion
598 from the atmosphere that balances the summer pCO_2 drawdown sustained by dilution
599 and primary production, and maintains sea ice pCO_2 above 100 ppm.
600 Despite the effect of snow and ice structure on fluxes, sea ice temperature appears to
601 exerts a crucial control on both sea ice pCO_2 gradient, gas transfer through permeability,
602 and ultimately on CO_2 transfer at the air-ice interface (fig 1b). We therefore derived an
603 empirical relationship between CO_2 flux and sea ice temperature (fig. 1b) allowing the
604 reconstruction of CO_2 flux fields (fig. 5) using sea ice temperature, concentration and
605 coverage from the NEMO-LIM3 large-scale sea ice-ocean model [*Madec*, 2008;
606 *Vancoppenolle et al.*, 2008]. Spring and summer air-ice CO_2 fluxes were estimated from
607 1997 to 2007 for non-flooded areas with ice concentration above 65% (fig. 6),
608 corresponding to the range of sea ice concentration encountered during sampling. This

609 up-scaling suggests that Antarctic sea ice cover pumps 0.029 PgC of atmospheric CO_2
610 (table 4) into the ocean during the spring-summer transition.
611 This assessment corroborates the first order independent assessment derived from pCO_2
612 dynamics relative to each main process (see previous section). Both CO_2 sink estimates
613 most probably underestimate the uptake of CO_2 over Antarctic sea ice as they do not
614 account for (1) areas with sea ice concentration < 65 %, (2) flooded areas, (3) surface
615 communities that may significantly enhance CO_2 uptake.

616

617 4. Conclusion

618 The elevated sea ice pCO_2 in winter results from an intricate superimposition of
619 counteracting processes: those increasing pCO_2 such as brine concentration and
620 carbonate precipitation, and those decreasing pCO_2 such as enhanced gas expulsion,
621 autumnal primary production, temperature decrease, CO_2 transfer to the gaseous phase.

622 In spring, we observed a sharp decrease of pCO_2 that is tightly related to sea ice melting
623 and related brine dilution. We also show that carbonate dissolution could induce pCO_2
624 changes comparable to those attributed to dilution. In summer, as sea ice becomes
625 isothermal, dilution effects level off. At that stage, uptake of atmospheric CO_2 and
626 mixing with underlying water (with pCO_2 values ranging from 380 to 430 ppm) should
627 maintain pCO_2 at or above the saturation level. However, sustained primary production
628 appears to be large enough to maintain low pCO_2 within the sea ice. One should note
629 that we did not address CO_2 uptake from the underlying to the ice driven by bottom
630 sympagic communities and CO_2 transfer from the underlying water to the atmosphere

631 through the ice that are considered insignificant [*Loose et al.*, 2011; *Rutgers van der*
632 *Loeff et al.*, 2014].

633 These processes act as sink for atmospheric CO_2. Using the relative contribution of the
634 main processes driving pCO_2 in sea ice we derived an uptake of 0.024 PgC for spring
635 and summer. This assessment corroborates the estimate from *in situ* CO_2 flux
636 measurements scaled with the ice temperature simulated with the NEMO-LIM3 model
637 that is assessed to 0.029 PgC. Both assessments compare favourably with the
638 assessments of *Rysgaard et al.* [2011] of 0.019 and 0.052 PgC yr^{-1} for the CO_2 fluxes
639 over the whole southern ocean, respectively "without" and "with"$CaCO_3$ formation in
640 sea ice.

641 We consider that the fluxes derived from the NEMO-LIM3 are the best estimate to date
642 of the uptake of atmospheric CO_2 by Antarctic sea ice in spring and summer.
643 Accordingly, sea ice provides an additional significant sink of atmospheric CO_2 in the
644 Southern Ocean up to 58 % of the estimated net uptake of the Southern Ocean south of
645 50°S (0.05 PgC yr^{-1}) [*Takahashi et al.*, 2009]. Antarctic pack ice appears to be a
646 significant contributor of CO_2 fluxes in the southern ocean. We believe that our
647 approach is conservative since we excluded areas with ice concentration below 65% and
648 flooded zones.

649

650 ## Acknowledgments

651 The authors appreciated the kindness and efficiency of the crews of *R.S.V Aurora*
652 *Australis, R.V. Polarstern and R.V. N.B.Palmer*. We are grateful to Tom Trull, Steve

Ackley and two anonymous reviewers for their useful comments that improved the quality of the manuscript. This research was supported by the Belgian Science Policy (BELCANTO projects, contract SD/CA/03A), the Belgian French Community (SIBCLIM project), the F.R.S.-FNRS and the Australian Climate Change Science Program. NXG received a PhD grant from the Fonds pour la Formation à la Recherche dans l'Industrie et l'Agriculture and now received financial support from the Canada Excellence Research Chair (CERC) program. BD is a research associate of the F.R.S.-FNRS. VS benefits from a COFUND Marie Curie fellowship "Back to Belgium Grant". Supplemental data used to produce figures are freely available at the address www.co2.ulg.ac.be/data/Delille_et_al_supplemental_data.xlsx. This is MARE contribution XXX.

References

Albert, M. R., A. M. Grannas, J. Bottenheim, P. B. Shepson, and F. E. Perron (2002), Processes and properties of snow-air transfer in the high Arctic with application to interstitial ozone at Alert, Canada, *Atmos. Environ.*, *36*(15-16), 2779-2787.

Albert, M. R., and F. E. Perron (2000), Ice layer and surface crust permeability in a seasonal snow pack, *Hydrological Processes*, *14*(18), 3207-3214.

Anderson, L. G., and E. P. Jones (1985), Measurements of total alkalinity, calcium and sulfate in natural sea ice, *J. Geophys. Res.*, *90*(C5), 9194-9198, doi:10.1029/JC090iC05p09194.

Arrigo, K. R. (2003), Primary production in sea ice, in *Sea ice: an introduction to its physics, chemistry, biology and geology*, edited by D. N. Thomas and G. Dieckmann, pp. 143-183, Blackwell Science, Oxford.

Arrigo, K. R., D. L. Worthen, M. P. Lizotte, P. Dixon, and G. Dieckmann (1997), Primary production in antarctic sea ice, *Science*, *276*, 394-397, doi:10.1126/science.276.5311.394.

Assur, A. (1958), Composition of sea ice and its tensile strength, in *Arctic Sea Ice*, edited, pp. 106-138, National Academy of Sciences-National Research Council.

Buckley, R. G., and H. J. Trodahl (1987), Thermally driven changes in the optical properties of sea ice, *Cold Reg. Sci. Technol.*, *14*(2), 201-204.

Burba, G., D. K. McDermitt, A. Grelle, D. J. Anderson, and L. Xu (2008), Addressing the influence of instrument surface heat exchange on the measurements of CO_2 flux

687 from open-path gas analyzers, *Global Change Biology*, *14*(8), 1854-1876,
688 doi:10.1111/j.1365-2486.2008.01606.x.
689 Comiso, J. C. (2003), Large-scale characteristics and variability of the global sea ice
690 cover, in *Sea ice: an introduction to its physics, chemistry, biology and geology*, edited
691 by D. N. Thomas and G. Dieckmann, pp. 112-142, Blackwell Science, Oxford.
692 Copin-Montégut, C. (1988), A new formula for the effect of temperature on the partial
693 pressure of carbon dioxide in seawater, *Mar. Chem.*, *25*(1), 29-37.
694 Cox, and W. Weeks (1983), Equations for determining the gas and brine volumes in
695 sea-ice samples, *J. Glaciol.*, *29*(102), 306-316.
696 Cox, G. F. N., and W. F. Weeks (1975), Brine drainage and initial salt entrapment in
697 sodium chloride ice*Rep.*, 85 pp. pp.
698 Delille, B., B. Jourdain, A. V. Borges, J. L. Tison, and D. Delille (2007), Biogas (CO_2,
699 O_2, dimethylsulfide) dynamics in spring Antarctic fast ice, *Limnol. Oceanogr.*, *52*(4),
700 1367-1379, doi:10.4319/lo.2007.52.4.1367.
701 Dickson, A. G., and F. J. Millero (1987), A comparison of the equilibrium constants for
702 the dissociation of carbonic acid in seawater media, *Deep-Sea Res. Part I Oceanogr.*
703 *Res. Pap.*, *34*, 1733-1743, doi:10.1016/0198-0149(87)90021-5.
704 Dieckmann, G. S., G. Nehrke, S. Papadimitriou, J. Göttlicher, R. Steininger, H.
705 Kennedy, D. Wolf-Gladrow, and D. N. Thomas (2008), Calcium carbonate as ikaite
706 crystals in Antarctic sea ice, *Geophys. Res. Lett.*, *35*(L08501),
707 doi:10.1029/2008GL033540.
708 Dieckmann, G. S., G. Nehrke, C. Uhlig, J. Göttlicher, S. Gerland, M. A. Granskog, and
709 D. N. Thomas (2010), Ikaite ($CaCO_3$*$6H_2O$) discovered in Arctic sea ice, *The*
710 *Cryosphere*, *4*(2), 227-230, doi:10.5194/tc-4-227-2010.
711 Eicken, H. (2003), From the microscopic, to the macroscopic, to the regional scale:
712 growth, microstructure and properties of sea ice, in *Sea ice: an introduction to its*
713 *physics, chemistry, biology and geology*, edited by D. N. Thomas and G. Dieckmann,
714 pp. 22-81, Blackwell Science, Oxford.
715 Frankignoulle, M. (1988), Field measurements of air-sea CO_2 exchange, *Limnol.*
716 *Oceanogr.*, *33*, 313-322.
717 Geilfus, N. X., G. Carnat, G. S. Dieckmann, N. Halden, G. Nehrke, T. Papakyriakou, J.
718 L. Tison, and B. Delille (2013), First estimates of the contribution of CaCO3
719 precipitation to the release of CO2 to the atmosphere during young sea ice growth,
720 *journal of geophysical Research - Oceans*, *118*(1-12), doi:10.1029/2012JC007980.
721 Geilfus, N. X., G. Carnat, T. Papakyriakou, J. L. Tison, B. Else, H. Thomas, E.
722 Shadwick, and B. Delille (2012), Dynamics of pCO_2 and related air-ice CO_2 fluxes in
723 the Arctic coastal zone (Amundsen Gulf, Beaufort Sea), *Journal of Geophysical*
724 *Research C: Oceans*, *117*(2), doi:10.1029/2011JC007118.
725 Gleitz, M., M. R. v.d.Loeff, D. N. Thomas, G. S. Dieckmann, and F. J. Millero (1995),
726 Comparison of summer and winter in organic carbon, oxygen and nutrient
727 concentrations in Antarctic sea ice brine, *Mar. Chem.*, *51*(2), 81-91, doi:10.1016/0304-
728 4203(95)00053-T.
729 Golden, K. M., S. F. Ackley, and V. I. Lytle (1998), The percolation phase transition in
730 sea ice, *Science*, *282*(5397), 2238-2241, doi:10.1126/science.282.5397.2238.
731 Gosink, T. A., J. G. Pearson, and J. J. Kelley (1976), Gas movement through sea ice,
732 *Nature*, *263*(2), 41-42, doi:10.1038/263041a0.
733 Gran, G. (1952), Determination of the equivalence point in potentiometric titration, part
734 II, *Analyst*, *77*, 661-671.

735 Haas, C., D. N. Thomas, and J. Bareiss (2001), Surface properties and processes of
736 perennial Antarctic sea ice in summer, *J. Glaciol.*, *47*(159), 613-625.
737 Haas, C., D. N. Thomas, and G. Dieckmann (2003), Dynamics versus thermodynamics:
738 the sea ice thickness distribution, in *Sea ice: an introduction to its physics, chemistry,*
739 *biology and geology*, edited, pp. 82-111, Blackwell Science, Oxford.
740 Hillebrand, H., C. D. Durselen, D. Kirschtel, U. Pollingher, and T. Zohary (1999),
741 Biovolume calculation for pelagic and benthic microalgae, *J. Phycol.*, *35*(2), 403-424,
742 doi:10.1046/j.1529-8817.1999.3520403.x.
743 Hunke, E. C., and J. K. Dukowicz (1997), An elastic-viscous-plastic model for sea ice
744 dynamics, *J Phys Oceanogr.*, *27*(9), 1849-1867, doi:10.1175/1520-
745 0485(1997)027<1849:AEVPMF>2.0.CO;2.
746 Johnson, K. M., et al. (1998), Coulometric total carbon dioxide analysis for marine
747 studies: assessment of the quality of total inorganic carbon measurements made during
748 the US Indian Ocean CO_2 Survey 1994-1996, *Mar. Chem.*, *63*(1-2), 21-37.
749 Jones, E. P., A. R. Coote, and E. M. Levy (1983), Effect of sea ice meltwater on the
750 alkalinity of sewater, *J. Mar. Res.*, *41*, 43-52.
751 Kalnay, E., et al. (1996), The NCEP/NCAR 40-year reanalysis project, *B Am Meteorol*
752 *Soc*, *77*(3), 437-471, doi:10.1175/1520-0477(1996)077<0437:TNYRP>2.0.CO;2.
753 Killawee, J. A., I. J. Fairchild, J. L. Tison, L. Janssens, and R. Lorrain (1998),
754 Segregation of solutes and gases in experimental freezing of dilute solutions:
755 Implications for natural glacial systems, *Geochim. Cosmochim. Acta*, *62*(23-24), 3637-
756 3655, doi:10.1016/S0016-7037(98)00268-3.
757 Lannuzel, D., V. Schoemann, I. Dumont, M. Content, J. de Jong, J.-L. Tison, B. Delille,
758 and S. Becquevort (2013), Effect of melting Antarctic sea ice on the fate of microbial
759 communities studied in microcosms, *Polar Biol.*, 1-15, doi:10.1007/s00300-013-1368-7.
760 Legendre, L., S. F. Ackley, G. S. Dieckmann, B. Gulliksen, R. Horner, T. Hoshiai, I. A.
761 Melnikov, W. S. Reeburgh, M. Spindler, and C. W. Sullivan (1992), Ecology of sea ice
762 biota 2. Global significance, *Polar Biol.*, *12*(3-4), 429-444.
763 Lewis, M. J. (2010), Antarctic snow and sea ice processes: effects on passive
764 microwave emissions and AMSR-E sea ice products, 224 pp, University of Texas at San
765 Antonio.
766 Lewis, M. J., J. L. Tison, B. Weissling, B. Delille, S. F. Ackley, F. Brabant, and H. Xie
767 (2011), Sea ice and snow cover characteristics during the winter–spring transition in the
768 Bellingshausen Sea: An overview of SIMBA 2007, *Deep-Sea Res. Oceanogr., II*, *58*(9–
769 10), 1019-1038, doi:10.1016/j.dsr2.2010.10.027.
770 Lizotte, M. P. (2001), The contributions of sea ice algae to Antarctic marine primary
771 production, *Am. Zool.*, *41*(1), 57-73, doi:10.1093/icb/41.1.57.
772 Lizotte, M. P., and C. W. Sullivan (1992), Biochemical-composition and photosynthate
773 distribution in sea ice microalgae of McMurdo-Sound, antarctica - evidence for nutrient
774 stress during the spring bloom, *Antarct. Sci.*, *4*(1), 23-30.
775 Loose, B., W. R. McGillis, P. Schlosser, D. Perovich, and T. Takahashi (2009), Effects
776 of freezing, growth, and ice cover on gas transport processes in laboratory seawater
777 experiments, *Geophys. Res. Lett.*, *36*, doi:10.1029/2008gl036318.
778 Loose, B., P. Schlosser, D. Perovich, D. B. Ringelberg, D. T. Ho, T. Takahashi, R.-M.
779 J., C. M. Reynolds, W. McGillis, and J. L. Tison (2011), Gas diffusion through
780 columnar laboratory sea ice: implications for mixed-layer ventilation of CO_2 in the
781 seasonal ice zone, *Tellus B*, *63*(B), doi:10.1111/j.1600-0889.2010.00506.x.

Madec, G. (2008), NEMO ocean engine, *Note du Pole de modélisation, Institut Pierre-Simon Laplace (IPSL), France*(27).
Massman, W. J., R. A. Sommerfeld, A. R. Mosier, K. F. Zeller, T. J. Hehn, and S. G. Rochelle (1997), A model investigation of turbulence-driven pressure-pumping effects on the rate of diffusion of CO_2 , N_2O, and CH_4 through layered snowpacks *Journal of Geophysical Research-Atmospheres*, *102*(D15), 18851-18863, doi:10.1029/97JD00844.
Massom, R. A., et al. (2006), ARISE (Antarctic Remote Ice Sensing Experiment) in the East 2003: Validation of satellite-derived sea-ice data products, *Annals of Glaciology*, *44*, 288-296.
Mehrbach, C., C. H. Culberson, J. E. Hawley, and R. M. Pytkowicz (1973), Measurements of the apparent dissociation constants of carbonic acid in seawater at atmospheric pressure, *Limnol. Oceanogr.*, *18*, 897-907.
Menden-Deuer, S., and E. J. Lessard (2000), Carbon to volume relationships for dinoflagellates, diatoms, and other protist plankton, *Limnol. Oceanogr.*, *45*(3), 569-579, doi:10.4319/lo.2000.45.3.0569.
Miller, L. A., T. N. Papakyriakou, R. E. Collins, J. W. Deming, J. K. Ehn, R. W. Macdonald, A. Mucci, O. Owens, M. Raudsepp, and N. Sutherland (2011), Carbon dynamics in sea ice: A winter flux time series, *J. Geophys. Res.*, *116*(C2), C02028, doi:10.1029/2009jc006058.
Mock, T. (2002), In situ primary production in young Antarctic sea ice, *Hydrobiologia*, *470*(1-3), 127-132.
Nicolaus, M., C. Haas, and S. Willmes (2009), Evolution of first-year and second-year snow properties on sea ice in the Weddell Sea during spring-summer transition, *Journal of Geophysical Research: Atmospheres*, *114*(D17), D17109, doi:10.1029/2008JD011227.
Nomura, D., H. Eicken, R. Gradinger, and K. Shirasawa (2010), Rapid Physically driven invesrion of the air-sea ice CO2 flux in the seasonal landfast ice off Barrow, Alaska after onset of surface melt, *Continental Shelf Research*, *30*(1), 1998-2004, doi:10.1016/j.csr.2010.09.014.
Nomura, D., M. Granskog, P. Assmy, D. Simizu, and G. Hashida (2013), Arctic and Antarctic sea ice acts as a sink for atmospheric CO2 during periods of snow melt and surface flooding, *Journal of Geophysical Research: Oceans*, *118*(12), 6511–6524, doi:10.1002/2013JC009048.
Notz, D., and M. G. Worster (2009), Desalination processes of sea ice revisited, *Journal of Geophysical Research: Oceans*, *114*(C5), C05006, doi:10.1029/2008JC004885.
Papadimitriou, S., H. Kennedy, G. Kattner, G. S. Dieckmann, and D. N. Thomas (2004), Experimental evidence for carbonate precipitation and CO_2 degassing during sea ice formation, *Geochim. Cosmochim. Acta*, *68*(8), 1749-1761, doi:10.1016/j.gca.2003.07.004.
Papadimitriou, S., H. Kennedy, P. Kennedy, and D. N. Thomas (2013), Ikaite solubility in seawater-derived brines at 1 atm and sub-zero temperatures to 265K, *Geochim. Cosmochim. Acta*, *109*(0), 241-253, doi:http://dx.doi.org/10.1016/j.gca.2013.01.044.
Papadimitriou, S., D. N. Thomas, H. Kennedy, C. Haas, H. Kuosa, A. Krell, and G. S. Dieckmann (2007), Biogeochemical composition of natural sea ice brines from the Weddell Sea during early austral summer, *Limnol. Oceanogr.*, *52*(5), 1809-1823, doi:10.4319/lo.2007.52.5.1809.
Papakyriakou, T. N., and L. A. Miller (2011), Springtime CO2 exchange over seasonal sea ice in the Canadian Arctic Archipelago, *Annals of Glaciology*, *52*, 215-224.

Poisson, A., and C. T. A. Chen (1987), Why is there little anthropogenic CO_2 in the Antarctic bottom water?, *Deep-Sea Res. Part A*, *34*(7), 1255-1275.
Redfield, A. C., B. H. Ketchum, F. A. Richards, and M. N. Hill (1963), The influence of organisms on the composition of sea-water, in *The composition of sea-water and comparative and descriptive oceanography*, edited, pp. 26-87, Wiley-Intersciences, New York.
Richards, F. A. (1965), Anoxic basins and fjords, edited by J. P. Riley and G. Skirrow, pp. 611-645, Academic Press, New York.
Richardson, C. (1976), Phase relatioships in sea ice as a function of temperature, *J. Glaciol.*, *17*, 507-519.
Rutgers van der Loeff, M. M., N. Cassar, M. Nicolaus, B. Rabe, and I. Stimac (2014), The influence of sea ice cover on air-sea gas exchange estimated with radon-222 profiles, *Journal of Geophysical Research: Oceans*, *119*(5), 2735-2751, doi:10.1002/2013JC009321.
Rysgaard, S., J. Bendtsen, B. Delille, G. S. Dieckmann, R. Glud, H. Kennedy, J. Mortensen, S. Papadimitriou, D. N. Thomas, and J. L. Tison (2011), Sea ice contribution to the air–sea CO2 exchange in the Arctic and Southern Oceans, *Tellus B*, doi:10.1111/j.1600-0889.2011.00571.x.
Rysgaard, S., R. N. Glud, K. Lennert, M. Cooper, N. Halden, R. J. G. Leakey, F. C. Hawthorne, and D. Barber (2012), Ikaite crystals in melting sea ice – implications for pCO2 and pH levels in Arctic surface waters, *The Cryosphere*, *6*(4), 901-908, doi:10.5194/tc-6-901-2012.
Rysgaard, S., R. N. Glud, M. K. Sejr, J. Bendtsen, and P. B. Christensen (2007), Inorganic carbon transport during sea ice growth and decay: A carbon pump in polar seas, *J. Geophys. Res., C*, *112*(C3), doi:doi:10.1029/2006jc003572.
Rysgaard, S., et al. (2013), Ikaite crystal distribution in winter sea ice and implications for CO2 system dynamics, *The Cryosphere*, *7*(2), 707-718, doi:10.5194/tc-7-707-2013.
Semiletov, I., A. Makshtas, S. I. Akasofu, and E. L. Andreas (2004), Atmospheric CO_2 balance: The role of Arctic sea ice *Geophys. Res. Lett.*, *31*(5), L05121-doi:05110.01029/02003GL017996.
Semiletov, I., I. Pipko, I. Repina, and N. Shakhova (2007), Carbonate chemistry dynamics and carbon dioxide fluxes across the atmosphere-ice-water interfaces in the Arctic Ocean: Pacific sector of the Arctic, *J. Marine Syst.*, *66*(1-4), 204-226, doi:10.1016/j.jmarsys.2006.05.012.
Søgaard, D., D. Thomas, S. Rysgaard, R. Glud, L. Norman, H. Kaartokallio, T. Juul-Pedersen, and N.-X. Geilfus (2013), The relative contributions of biological and abiotic processes to carbon dynamics in subarctic sea ice, *Polar Biol.*, *36*(12), 1761-1777, doi:10.1007/s00300-013-1396-3.
Takagi, K., M. Nomura, D. Ashiya, H. Takahashi, K. Sasa, Y. Fujinuma, H. Shibata, Y. Akibayashi, and T. Koike (2005), Dynamic carbon dioxide exchange through snowpack by wind-driven mass transfer in a conifer-broadleaf mixed forest in northernmost Japan, *Global Biogeochem. Cycles*, *19*(2), doi:10.1029/2004GB002272.
Takahashi, T., et al. (2009), Climatological Mean and Decadal Change in Surface Ocean pCO_2, and Net Sea-air CO_2 Flux over the Global Oceans, *Deep-Sea Res. Oceanogr., II*, *56*(8-10), 554-577, doi:10.1016/j.dsr2.2008.12.009.
Thomas, D. N., and G. S. Dieckmann (2002), Biogeochemistry of Antarctic sea ice, *Oceanogr. Mar. Biol.*, *40*, 143-169.

877 Timmermann, R., H. H. Hellmer, and A. Beckmann (2002), Simulations of ice-ocean
878 dynamics in the Weddell Sea 2. Interannual variability 1985-1993, *J. Geophys. Res.*,
879 *107*(C3), 11.11-11.19, doi:10.1029/2000JC000742.
880 Tison, J. L., C. Haas, M. M. Gowing, S. Sleewaegen, and A. Bernard (2002), Tank
881 study of physico-chemical controls on gas content and composition during growth of
882 young sea ice, *J. Glaciol.*, *48*(161), 177-191.
883 Tison, J. L., A. Worby, B. Delille, F. Brabant, S. Papadimitriou, D. Thomas, J. de Jong,
884 D. Lannuzel, and C. Haas (2008), Temporal evolution of decaying summer first-year
885 sea ice in the Western Weddell Sea, Antarctica, *Deep-Sea Res. Oceanogr., II*, *55*(8-9),
886 975-987, doi:doi:10.1016/j.dsr2.2007.12.021.
887 Vancoppenolle, M., C. M. Bitz, and T. Fichefet (2007), Summer landfast sea ice
888 desalination at Point Barrow, Alaska: Modeling and observations, *J. Geophys. Res., C*,
889 *112*(C4), -, doi:10.1029/2006jc003493.
890 Vancoppenolle, M., T. Fichefet, H. Goosse, S. Bouillon, G. Madec, and M. A. M.
891 Maqueda (2008), Simulating the mass balance and salinity of Arctic and Antarctic sea
892 ice. 1. Model description and validation, *Ocean Model.*, *27*(1-2), 33-53,
893 doi:10.1016/j.ocemod.2008.10.005.
894 Wadhams, P., M. A. Lange, and S. F. Ackley (1987), The ice thickness distribution
895 across the atlantic sector of the antarctic ocean in midwinter, *J. Geophys. Res.*, *92*(C13),
896 14535-14552.
897 Weeks, W. F., and S. F. Ackley (1986), The growth, structure and properties of sea ice,
898 in *The growth, structure and properties of sea ice*, edited by N. Untersteiner, pp. 9-164,
899 Plenum Press, New York.
900 Weiss, R. F. (1987), Winter Weddell Sea Project 1986: Trace gas studies during legs
901 ANT V/2 and ANT V/3 of Polarstern, *Antarct. J. U.S.*, *22*, 99-100.
902 Weiss, R. F., H. G. Ostlund, and H. Craig (1979), Geochemical studies of the Weddell
903 sea, *Deep-Sea Res. Part I*, *26*, 1093-1120, doi:10.1016/0198-0149(79)90059-1.
904 Wettlaufer, J. S., M. G. Worster, and H. E. Huppert (1997), Natural convection during
905 solidification of an alloy from above with application to the evolution of sea ice, *J.*
906 *Fluid Mech.*, *344*, 291-316, doi:10.1017/S0022112097006022.
907 Zemmelink, H. J., B. Delille, J. L. Tison, E. J. Hintsa, L. Houghton, and J. W. H. Dacey
908 (2006), CO_2 deposition over the multi-year ice of the western Weddell Sea, *Geophys.*
909 *Res. Lett.*, *33*(13), doi:L13606, doi:10.1029/2006gl026320.
910 Zhou, J., B. Delille, H. Eicken, M. Vancoppenolle, F. Brabant, G. Carnat, N.-X. Geilfus,
911 T. Papakyriakou, B. Heinesch, and J.-L. Tison (2013), Physical and biogeochemical
912 properties in landfast sea ice (Barrow, Alaska): Insights on brine and gas dynamics
913 across seasons, *Journal of Geophysical Research: Oceans*, 3172-3189,
914 doi:10.1002/jgrc.20232.
915

916

Table 1: Fit expression of the relationship between CO_2 fluxes (F_{CO2}) over both first year and multiyear ice as a function of sea ice temperature (T_{si}) at 5cm depth used for reconstructing air-ice CO_2 fluxes from the NEMO-LIM3 model as it appears in figure 1b (solid curve). Number of samples, mean error, standard error, root-mean-square error, coefficient of determination were 21, -0.099 mmol C m^{-2} d^{-1}, 0.995 mmol C m^{-2} d^{-1}, 0.953, 0.728, respectively.

T_{si} (°C)	F_{CO2} (mmol C m^{-2} d^{-1})
$T_{si} < -9$	0
$-9 < T_{si} < -7$	$F_{CO2}=27.945 + 6.39\ T_{si} + 0.365\ T_{si}^2$
$T_{si} > -7$	$F_{CO2}=-4.41962 - 0.54286\ T_{si}\ 0.035\ T_{si}^2$

Table 2: Estimates of potential pCO_2 changes related to spring and summer physical and biogeochemical processes observed during the 2003/V1 and ISPOL cruises.

	related changes						
	Temperature (°C)	Salinity (of brines)	TA (µmol kg^{-1} of bulk ice)	DIC (µmol kg^{-1} of bulk ice)	TA (µmol kg^{-1} of brines)	DIC (µmol kg^{-1} of brines)	pCO_2 (ppm in brines)
temperature increase and related dilution	5.9	-94	0	0	-2125	-1813	-684
Primary production	0	0	4.1	-25.8	107	-669	-639
$CaCO_3$ dissolution	0	0	157.2	78.6	4075	2038	-583

Table 3: Estimates of potential air-ice CO_2 fluxes in order to restore equilibrium following changes in brine pCO_2 associated to spring and summer physical and biogeochemical processes observed during the 2003/V1 and ISPOL cruises. Flux representative of a 4 month period.

process	related CO_2 transfer from the atmosphere (mmol m^{-2})
temperature increase and related dilution	-60
$CaCO_3$ dissolution	-57
Primary production	-25
Total	-141

938 Table 4: Spring and summer air-ice CO_2 fluxes assessed with the NEMO-LIM3 model

939 from 1997 to 2009

year	Total CO_2 sink (PgC)
1997	-0.0273
1998	-0.0272
1999	-0.0289
2000	-0.0301
2001	-0.0274
2002	-0.0301
2003	-0.0299
2004	-0.0293
2005	-0.0298
2006	-0.0287
2007	-0.0291
mean	-0.0289
STD	0.0011

940

941 **Figures**

942 Figure 1: (a) pCO_2 within brines ($pCO_{2\ brines}$) versus sea ice temperature integrated over
943 the depth of sackholes (green: 2003/V1cruise, orange: ISPOL cruise, blue: SIMBA
944 cruise). Grey triangles correspond to two stations carried out on a snow loaded floe
945 which experienced flooding. Horizontal dotted line and solid curve are pCO_{2air} and the
946 regressed $pCO_{2\ brine}$, respectively. Fit expression of the regressed pCO_2 brine as a
947 function of sea ice temperature (T_{si}) is: $pCO_{2\ brine} = 101.5 + 12.96\ T_{si} + 3.915\ T_{si}^2 - 1.360\ T_{si}^3$ (number of points analysed and coefficient of determination are 65 and 0.8625,
948
949 respectively). Red dashed curve represents the theoretical variation related to both
950 dilution and the thermodynamic effect of temperature increase (see text for details). (b)
951 Net air-sea ice CO_2 fluxes versus snow-ice interface temperature. Solid curve
952 represents the relationship of air- ice CO_2 fluxes to snow-ice interface temperature used
953 for reconstructing air-ice CO_2 fluxes from the NEMO-LIM3 model. Flux measurements
954 during superimposed ice events (grey diamonds) were excluded from the calculation.
955 Correspondence between season and ice temperature is only indicative and corresponds
956 to the conditions encountered during our surveys.

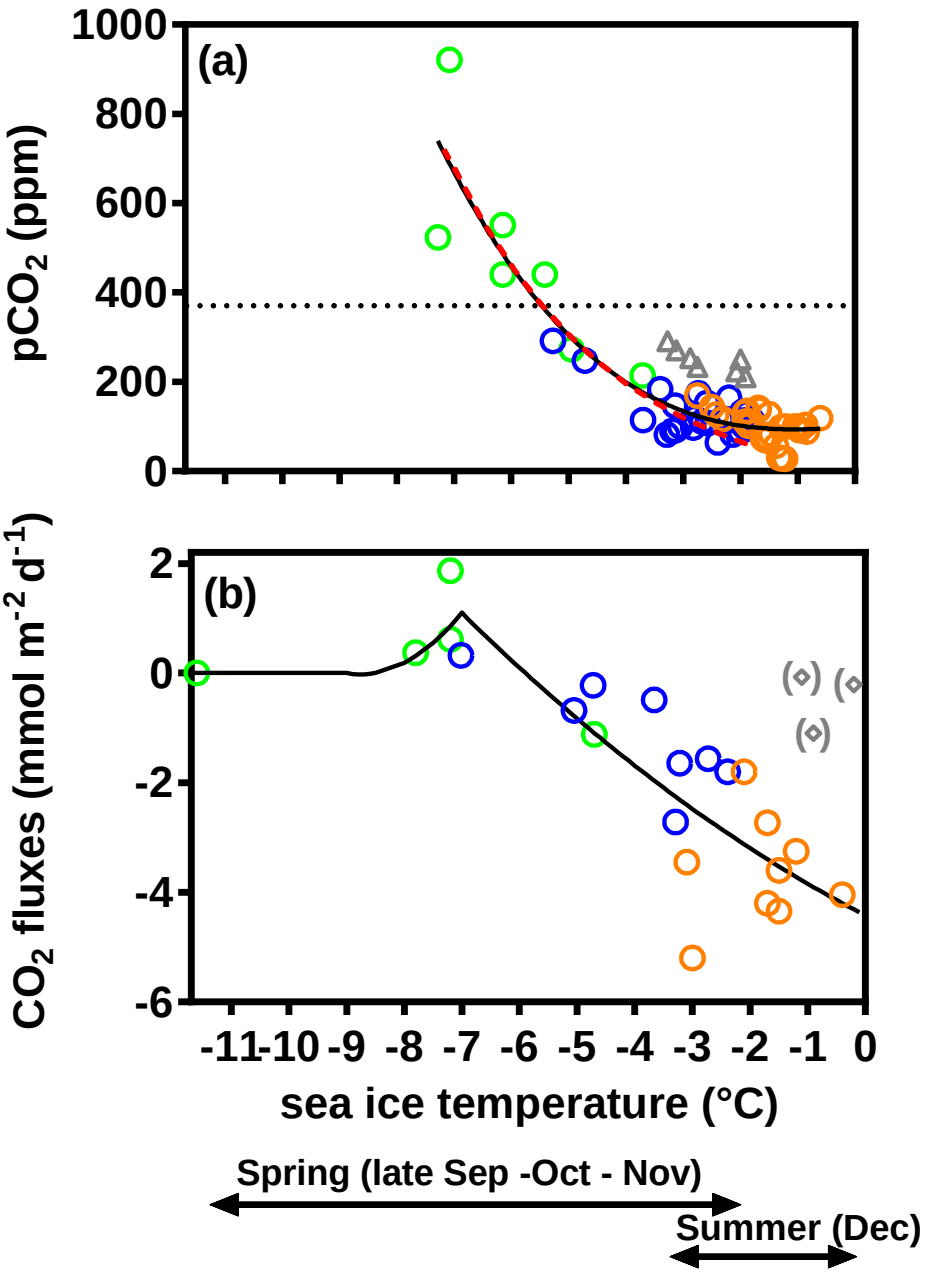
(a)
1000
800
600
400
200
0
pCO2 (ppm)
(b)
2
0
-2
-4
-6
CO2 fluxes (mmol m-2 d-1)
-11 -10 -9 -8 -7 -6 -5 -4 -3 -2 -1 0
sea ice temperature (°C)
Spring (late Sep -Oct - Nov)
Summer (Dec)

957

958

959 Figure 2: Scheme of the representation of sea ice in the LIM3 model, showing the L=5
960 thickness categories, horizontally uniform with unique ice thickness (hil) and snow
961 depth (hsl) and characterized by a relative coverage a^l. In each ice thickness category,
962 the snow-ice column is vertically divided into one layer of snow and N=5 layers of sea
963 ice.

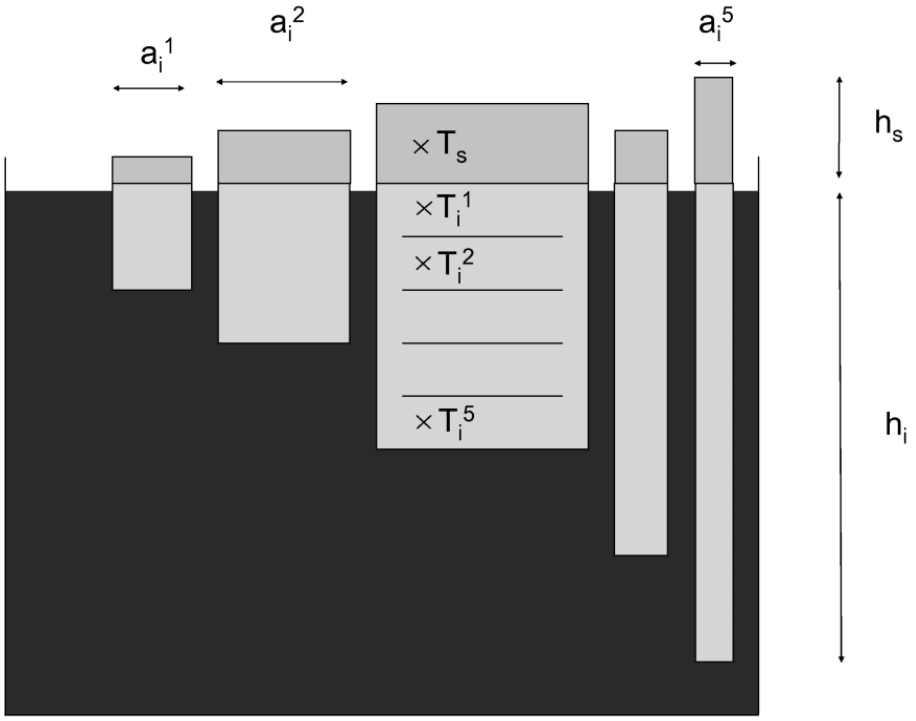

964
965
966
967

Figure 3: Normalized DIC to a constant salinity of 35 (DIC_{35}) against normalized TA (TA_{35}). Open squares and open circles denote spring (2003/V1 cruise) and summer (ISPOL cruise) samples, respectively. The slope of the corresponding regression line is reported as "α". Solid square and circle report the average of all under-ice measurements carried during 2003/V1 and ISPOL cruise, respectively (the corresponding average pCO_2 are 417 and 390 ppm, respectively). Arrows represent the theoretical variation of DIC_{35} and TA_{35} due to biogeochemical processes (i,e, photosynthesis/respiration, calcium carbonate dissolution/precipitation, mixing with underlying water, uptake/release of CO_2 with the atmosphere or bubbles trapped within the ice). The theoretical slopes of the relative variation of TA35 and DIC35 of each biogeochemical process are given (number between brackets).

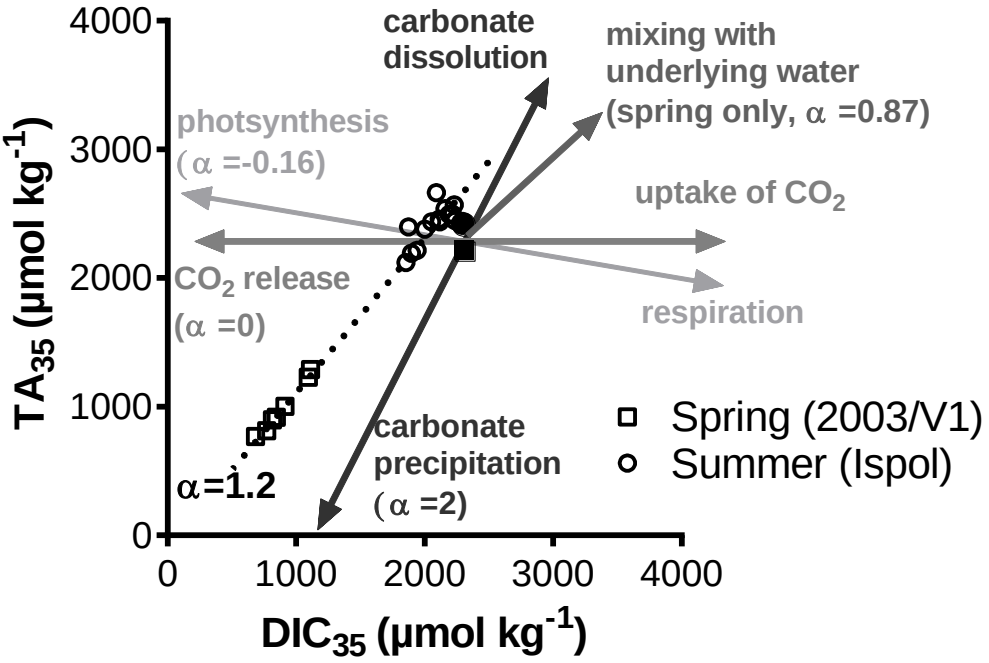

982 Figure 4: Fate of carbonate solids precipitated within sea ice

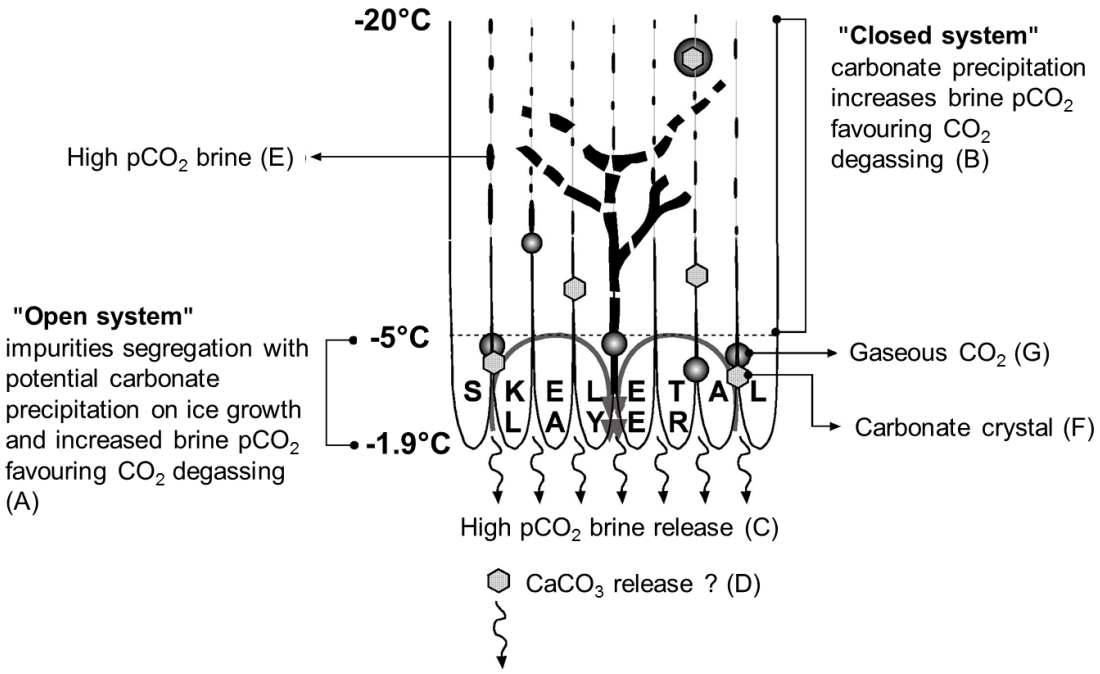

983

984

985 Figure 5: Distribution of the ice-air CO_2 flux (mmolC m^{-2} d^{-1}) over the Antarctic sea ice
986 zone, in September 2003 (A, corresponding to the period of the 2003/V1 cruise) and in
987 December 2004 (B, corresponding to the period of the ISPOL cruise), reconstructed
988 from ice temperature simulated by NEMO-LIM3 model, for ice concentrations >
989 65%.

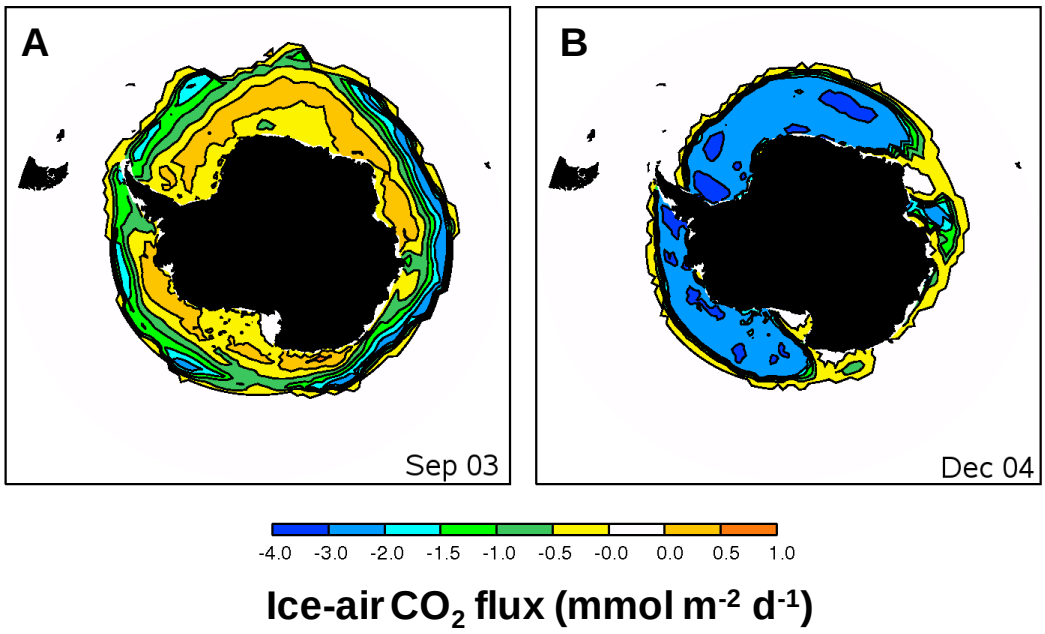

990

991

992 Figure 6: Average September to December distribution of the ice-air CO_2 flux over the
993 Antarctic sea ice zone (mmolC m^{-2} d^{-1}) as simulated by the sea ice model, during the
994 1997-2007.

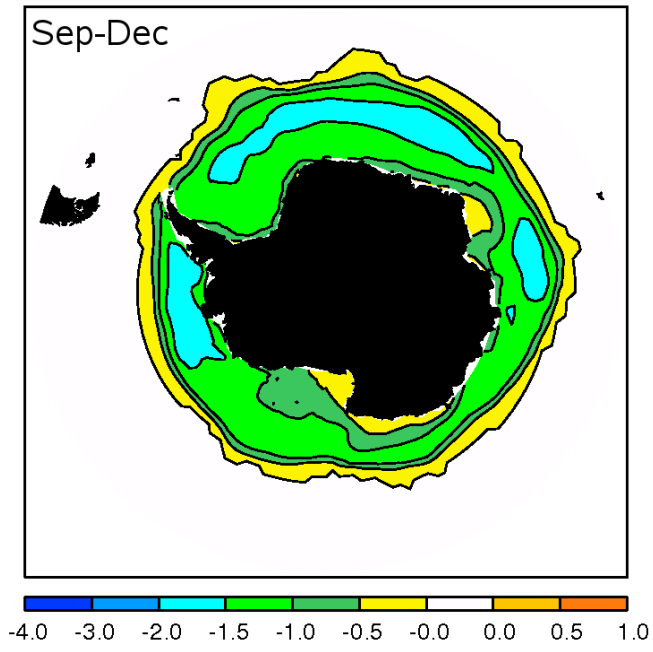

995

996